AGU PUBLICATIONS

JGR

Journal of Geophysical Research: Oceans

RESEARCH ARTICLE

10.1002/2014JC010067

Special Section:
Early scientific results from the salinity measuring satellites Aquarius/SAC-D and SMOS

Quality assessment of spaceborne sea surface salinity observations over the northern North Atlantic

Julia Köhler[1], Meike Sena Martins[1], Nuno Serra[1], and Detlef Stammer[1]

[1]Centrum für Erdsystemforschung und Nachhaltigkeit, Universität Hamburg, Hamburg, Germany

Key Points:
- Satellite SSS fields show realistic spatial SSS distribution
- SST-dependent bias in the SMOS retrieval
- Differences to observations can partially be attributed to frontal processes

Correspondence to:
J. Köhler,
julia.koehler@zmaw.de

Citation:
Köhler, J., M. Sena Martins, N. Serra, and D. Stammer (2015), Quality assessment of spaceborne sea surface salinity observations over the northern North Atlantic, *J. Geophys. Res. Oceans*, *120*, 94–112, doi:10.1002/2014JC010067.

Received 17 APR 2014
Accepted 15 DEC 2014
Accepted article online 23 DEC 2014
Published online 19 JAN 2015

Abstract Spaceborne sea surface salinity (SSS) measurements provided by the European Space Agency's (ESA) "Soil Moisture and Ocean Salinity" (SMOS) and the National Aeronautical Space Agency's (NASA) "Aquarius/SAC-D" missions, covering the period from May 2012 to April 2013, are compared against in situ salinity measurements obtained in the northern North Atlantic between 20°N and 80°N. In cold water, SMOS SSS fields show a temperature-dependent negative SSS bias of up to −2 g/kg for temperatures <5°C. Removing this bias significantly reduces the differences to independent ship-based thermosalinograph data but potentially corrects simultaneously also other effects not related to temperature, such as land contamination or radio frequency interference (RFI). The resulting time-mean bias, averaged over the study area, amounts to 0.1 g/kg. A respective correction applied previously by the Jet Propulsion Laboratory to the Aquarius data is shown here to have successfully removed an SST-related bias in our study area. For both missions, resulting spatial structures of SSS variability agree very well with those available from an eddy-resolving numerical simulation and from Argo data and, additionally they also show substantial salinity changes on monthly and seasonal time scales. Some fraction of the root-mean-square difference between in situ, and SMOS and Aquarius data (approximately 0.9 g/kg) can be attributed to short time scale ocean processes, notably at the Greenland shelf, and could represent associated sampling errors there.

1. Introduction

Variations of salinity play an important role in the ocean. They are an expression of varying freshwater transports and their convergences and as such are a diagnostic of the ocean's role in the global hydrological cycle. On the other hand, salinity, through its impact on density, influences the ocean circulation and thereby plays an active role in shaping climate change. Quantifying salinity variations in the ocean and understanding their underlying processes therefore has to be considered a fundamental problem of physical oceanography. Nevertheless, salinity is historically one of the notoriously undersampled variables of the time-varying ocean state, leaving a detailed knowledge about long-term ocean salinity changes still elusive.

In general terms, variations of salinity can result from a changing ocean circulation, and through vertical mixing processes and associated exchanges of freshwater and salt, especially between the surface and subsurface layers. On the surface, salinity fields can generally also change in response to geographically and temporally varying net surface freshwater fluxes, resulting from the sum of precipitation (P) and evaporation (E) over the ocean plus continental discharge (R), as well as sea ice and land ice melting [*Yu*, 2011]. In particular at high-latitudes, freshwater sources can also originate from melting of land and sea ice and changes in freshwater transports by ocean currents which have likely contributed to observed salinity changes there as well [e.g., *Polyakov et al*., 2008; *Jacobs and Giulivi*, 2010].

Today two recent technological advances fundamentally improve the basis of salinity measurements, finally enabling oceanographers to investigate contemporary salinity variations and their relation to the global hydrological cycle. The first such advancement resulted from the advent of the global Argo float array, which, since 2002, for the first time in history, globally provides vertical profiles of salinity observations every 10 days for the top 2000 m with a nominal spatial coverage of 3°. Based on these novel data, *Durack and Wijffels* [2010] and *Hosoda et al*. [2009] reported an increase of surface salinity in evaporation-dominated regions and a decrease in precipitation-dominated regions, consistent with an amplification of the global hydrological cycle [*Helm et al*., 2010].

The second major advancement in observing ocean salinity came about through the launch of two satellite missions designed to measure sea surface salinity (SSS) from space. The first mission, the European Space

Agency's (ESA) SMOS ("Soil Moisture and Ocean Salinity") [*Font et al*., 2004] started retrieving SSS in November 2009, followed, 2 years later, by the American National Aeronautical Space Agency's (NASA) "Aquarius/SAC-D" mission [*Lagerloef et al*., 2008]. From both missions, SSS data are now available on a routine basis, covering the global ocean every 3 (SMOS) or 7 (Aquarius) days with a spatial resolution of roughly 40 km for SMOS and 100 km for Aquarius. Significant benefits can be expected from these novel satellite SSS fields for quantitative studies of ocean salinity variations. However, before their full potential can unfold, they need to be tested and improved through a detailed intercomparison of satellite retrievals with in situ data.

By now, few such validation tests of SMOS and Aquarius SSS data are available. However, most of these studies focus on warm waters with large salinity signals (spatially and/or temporally), e.g., the Amazon River freshwater plume [*Reul et al*., 2013]. *Banks et al*. [2012] validated first SMOS SSS retrievals in the Atlantic Ocean using Argo and model data. More recently, *Boutin et al*. [2013] examined the impact of rain on sea surface freshening and compared SMOS and Argo measurements in the high-precipitation region of the Pacific Ocean's Inter-Tropical Convergence Zone. Using Aquarius data, *Lee et al*. [2012] studied dynamical SSS features in the eastern equatorial Pacific associated with tropical instability waves. Moreover, modern surface drifter measurements of near-surface salinity in the top 50 cm and SMOS measurements were compared in high precipitation and tropical regions remote from any land contamination [*Morisset et al*., 2012].

The present note aims to fill an important gap in validation studies by testing SMOS and Aquarius SSS retrievals against in situ salinity observations obtained over regions of cold waters in the subpolar North Atlantic and Nordic Seas during a series of observational cruises from aboard German and Scandinavian research vessels conducted in the Irminger, Norwegian, and Iceland Seas. Jointly with results from an eddy-resolving (4 km nominal spatial resolution) model simulation of the North Atlantic and Arctic, we will use these high-quality in situ salinity measurements to demonstrate that SMOS and Aquarius satellite data are capable of documenting spatial variations in surface salinity, even in cold water. Aided by model simulations, differences between in situ salinity measurements and satellite salinity retrievals will be interpreted in terms of uncertainties in the retrievals (in particular temperature-dependent uncertainties), but also in terms of processes leading to temporal variability and vertical salinity gradients in the ocean.

The structure of the remaining paper is as follows: in section 2, we will briefly summarize the methodology and data used. The bias in salinity satellite retrievals, as observed in the North Atlantic, is estimated in section 3. Section 4 makes use of the model simulation to formulate hypotheses for differences between satellite and in situ observations and potential error sources are discussed. Section 5 compares corrected SSS fields with in situ data and in section 6, the available information is used to quantify salinity variations in the Atlantic during the course of one annual cycle. Section 7 provides concluding remarks and an outlook.

2. Methodology

In this section, we will first summarize the SMOS and Aquarius salinity retrievals and explain differences between both missions, to the extent that they are relevant for this study. We will subsequently summarize other data sets used, notably ship-based thermosalinograph (TSG) measurements and Argo data. We will also describe the configuration of the eddy-resolving model of the Arctic-North Atlantic Oceans, which aids our analysis.

2.1. SMOS SSS Retrievals

With its Microwave Imaging Radiometer using Aperture Synthesis (MIRAS) instrument, measuring the microwave radiation emitted from the earth's surface in the 1.4 GHz L-Band range, ESA's SMOS mission pioneers a completely new synthetic aperture antenna technique to measure ocean surface salinity. The new technique requires the space-time inversion of measurements made from 69 small antennas during 1.2 s time frames arranged along Y-shaped antenna arms [*McMullan et al*., 2008]. The resulting field of view (FOV) of the satellite covers a swath of about 1000 km in width, over which MIRAS features a spatial resolution, ranging from 35 km in the center to about 80 km near the swath edges.

SMOS Level 2 salinity products are available from year 2010 onward. However, because of problems with the SMOS SSS retrieval, especially those related to radio frequency interference (RFI) caused by ground-based L-band radiation sources, data remain corrupted, especially in the North Atlantic before May 2012, when major RFI sources on Canada and Greenland were finally switched off [*ESA*, 2012]. However, RFI

remains a problem in many areas including parts of the Atlantic, but is now more subtle and therefore less easy to detect and to eliminate.

Presently, Level 3 and Level 4 SMOS SSS products (L3 and L4 henceforth) are available from the Barcelona Expert Centre (BEC), which are based on the ESA's Level 2 (L2), Ocean Salinity User Data Product (UDP), and Ocean Salinity Data Analysis Product (DAP). Before BEC creates the L3 and L4 products—all of which are based on the SMOS Semi-Empirical Ocean Forward Model [*Guimbard et al*., 2012]—geographical, retrieval, and geometrical filters are applied to the reprocessed L2 data [*SMOS-BEC Team*, 2014]. As an example, data with suspected ice presence or contamination by RFI (>33%) were eliminated from further processing. For a detailed filter and product description, see *SMOS-BEC Team* [2014]; also described therein is the L3 product, called binned product, which is constructed by weighted averaging of the filtered reprocessed L2 data.

Our study is based on the L4 product, which was constructed by fusing the L3 binned maps using the singularity analysis technique [*Turiel et al*., 2009; *Umbert et al*., 2014] applied to the high-resolution Ostia sea surface temperature (SST) fields [*Donlon et al*., 2012]. As explained by *Umbert et al*. [2014], singularity analysis is a technique suited for estimating the singularity exponents of a signal which characterizes the presence of ocean structures in different scalars. The method is especially useful to assess the geographical consistency of remote sensing variables [*Umbert et al*., 2014]. Although this technique does not attempt to correct for biases, regional structures are better preserved, which is of importance especially in frontal areas. The monthly SSS fields are available on a $0.25^\circ \times 0.25^\circ$ grid and can be downloaded at http://cp34-bec.cmima.csic.es/ocean-reprocessed-dataset. We linearly interpolated the L4 product as monthly means onto a $1^\circ \times 1^\circ$ spatial grid.

In the following, data from ascending and descending SMOS arcs will be analyzed separately, because we anticipated differences in their data quality and in their error characteristics. In particular, we expected significant differences in the quality of the data from both arcs due to higher influence of the ocean-land transition, remaining RFI sources and sun activity, which in the Atlantic degrade especially data from descending orbits [*Martinez*, 2013]. As explained by *Font et al*. [2013] and by *Gabarro et al*. [2012], contamination from continents is still a problem when land masses enter the very wide SMOS antenna FOV. Within a band of 1500 km around the main continental masses and sea ice boundaries, absolute salinity values therefore have to be treated with caution [*Gabarro et al*., 2012]. Efforts are underway to further characterize and remove the land-sea contamination over the ocean (J. Tenerelli, personal communication, and the SMOS Quality Working Group Nr.14, 2014).

Figures 1a and 1b show the monthly averaged data availability for SMOS ascending and descending orbits during the study period of May 2012 to April 2013. Most of the North Atlantic is, with 12 values per grid box, fully covered during the study period. Exceptions can be found near the eastern Greenland coast due to ice cover and in the vicinity of the European continent due to land and/or ice contamination. Remaining active RFI sources from Northern Europe lead to a reduced data availability closer to the coasts [*Daganzo-Eusebio et al*., 2013], especially for the descending arcs, for which the European continent is getting into the FOV. Data near the coast are contaminated by land effects, e.g., in the European North Sea (Figure 1b).

2.2. Aquarius SSS Retrievals

The NASA's Aquarius satellite directly retrieves brightness temperatures using three horn-antennas, which provide three beams viewing three spatially displaced regions with a slightly different footprint size. In contrast to the SMOS mission, for which sea surface roughness is estimated from additional wind fields (ECMWF 10 m equivalent neutral wind data are used as auxiliary data in the SMOS L2 processing to improve the retrievals which is performed through a multiparametric inversion scheme based on a minimization of a maximum-likelihood Bayesian-based cost function [*Gabarro et al*., 2009]), Aquarius carries an active scatterometer, measuring the roughness instantaneously over the satellite footprint. Like SMOS, Aquarius SSS fields also suffer from land contamination, but as its FOV is much smaller (using only instantaneous data), the land contamination is reduced to a region of about 150 km in width around continental margins [*Kim et al*., 2014]. Even though the FOV is smaller for Aquarius than for SMOS, the SMOS resolution is higher due to the interferometric principle of the 69 small antennas. Aquarius reaches global coverage after 7 days and the spatial resolution is about 100 km.

In this study, we use monthly Aquarius SSS retrievals available on a $1^\circ \times 1^\circ$ grid for the period May 2012 to April 2013. These fields are based on the recent Aquarius V3 product (version 3.0, $SSS_{bias-adj}$), which was

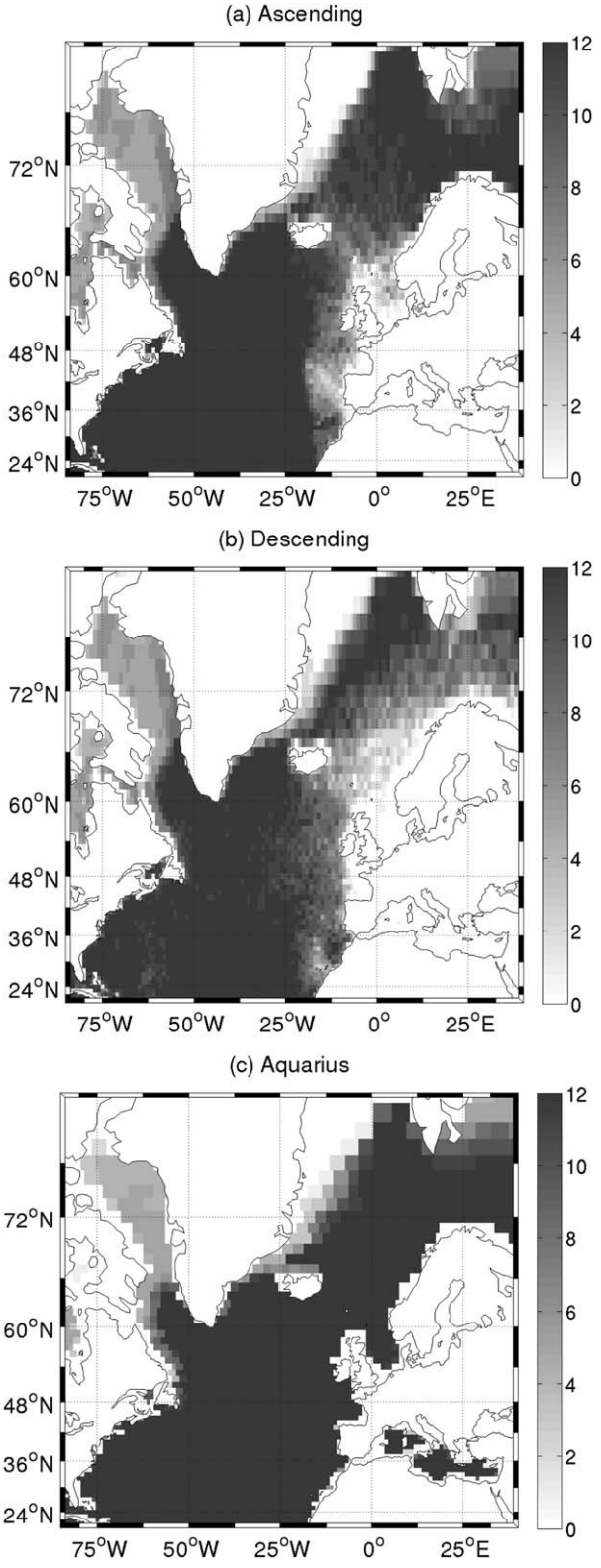

Figure 1. Data product availability (in months) during May 2012 to April 2013 for (a) SMOS SSS from ascending orbits, (b) SMOS SSS from descending orbits, and (c) Aquarius SSS.

retrieved from ftp://podaac-ftp.jpl.nasa.gov/allData/aquarius/L3/mapped/V3/monthly/SCISM. The changes made between the V2.0 and V3.0 products are documented in *Meissner et al.* [2014] (ftp://podaac-ftp.jpl.nasa.gov/allData/aquarius/docs/v3) and include an update of the antenna pattern coefficients, the use of Aquarius-derived wind speeds in the roughness correction and an empirical correction to the reflected galactic radiation, which reduces the bias between ascending and descending passes. New in the V3.0 fields is also the removal of a SST-related SSS bias [*Meissner et al.*, 2014], which is not unlike of what is being discussed here in our analysis. The data availability of Aquarius (Figure 1c) is close to 12 values per grid box except around Greenland and east of Spitsbergen.

2.3. Ship-Based Thermosalinograph Data

Ship-based thermosalinograph (TSG) salinity measurements were acquired simultaneously to SMOS and Aquarius measurements from aboard the German research vessels RV "Poseidon" (cruises P437-1 and P437-2) and RV "Maria S. Merian" (cruises MSM21-1, MSM21-3, and MSM27), as well as from aboard the Norwegian RV "Johan Hjort" and RV "G.O. Sars"; the latter data were provided by the Norwegian Marine Data Centre. All research vessels operated in the subpolar North Atlantic and Nordic Seas during the period from May 2012 to April 2013 (except for January 2013); Figure 2a shows all respective cruise tracks from which data are used in this study.

As a first analysis step, the 1 Hz TSG measurements were calibrated using bottle data and CTD measurements available in a 4–8 m depth range, within which the TSG measurements were obtained. An example of the resulting TSG salinity variations is shown in Figure 2b jointly with the CTD measurements used for calibration of the TSG salinity. A comparison involving all data reveals an accuracy of the point-wise TSG data of 0.005 g/kg at the depth of the measurement where the ships' hull water intake

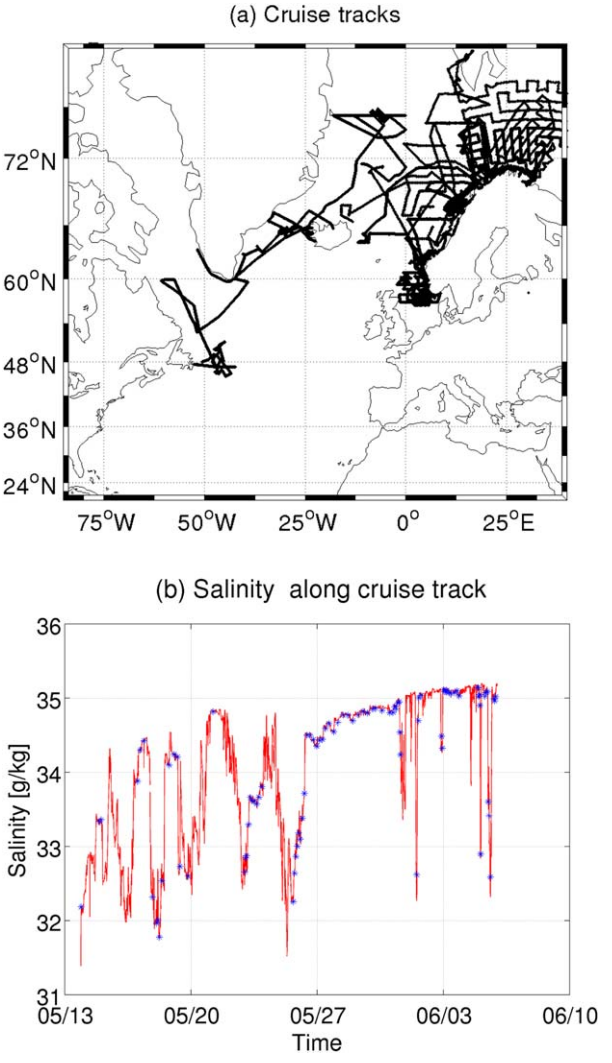

Figure 2. (a) Cruise tracks along which in situ thermosalinograph data were collected. (b) Thermosalinograph salinity measured during May 2012 along one cruise track of the German R/V "Maria S. Merian" (solid line). CTD measurements used for calibration of the thermosalinograph data are shown with asterisks.

occurs. For a comparison with the satellite data, TSG observations were averaged within the same $1^\circ \times 1^\circ \times 1$ month grid cells for which SMOS and Aquarius data are available. For the later interpretation of the results, we note, however, that SMOS measurements represent the salinity values of the top centimeter of the sea surface whereas the TSG measurements originate from 4 to 8 m depth levels.

2.4. Argo Data Set

For validation purposes, we used gridded $1^\circ \times 1^\circ$ salinity fields constructed from Argo measurements obtained during the period May 2012 to April 2013 in the North Atlantic between 20°N and 80°N and available as delayed mode and quality controlled Argo profile data via ftp://ftp.ifremer.fr/ifremer/argo/etc/geo. From each Argo profile, we extracted the uppermost salinity value located between 4 and 12 dbar; of those data, 84% correspond to a depth between 4 and 6 m. Additional quality checks were applied subsequently to check for static stability within each profile and to exclude data exceeding 3 times the standard deviation from the WOA09 climatology (a criteria which excludes about 1% of the data).

2.5. Eddy-Resolving Numerical Simulation

The interpretation of the SMOS and Aquarius fields is aided in this study by using the output from an eddy-resolving numerical circulation model of the North Atlantic and Arctic circulations. The model is based on the Massachusetts Institute of Technology (MIT) general circulation model [*Marshall et al*., 1997b] and was configured for the Atlantic Ocean north of 33°S, including the Mediterranean and Baltic Seas, the Nordic Seas and the Arctic Ocean, as described in *Serra et al*. [2010]. It was run here at the resolution of about 4 km (the equivalent of a 1/24° spatial resolution in the equator). The vertical discretization (with 100 vertical levels) varies from 5 m in the upper 200 m ocean to 275 m in the deep ocean. The model bottom topography was extracted from ETOPO2 and the initial temperature and salinity conditions were obtained from another run performed with a 8 km spatial resolution and which started (in January 1948) from the WOA09 climatology.

The model is forced at the surface by fluxes of momentum, heat, and freshwater computed using bulk formulae and the 6 hourly atmospheric state from the ECMWF/ERA-interim Reanalysis [*Dee et al*., 2011]. During the run, the model sea surface salinity is weakly relaxed to the Polar Science Center Hydrographic Climatology 3.0 [*Steele et al*., 2001] with a relaxation time scale of 1 month. At the volume-balanced open northern and southern boundaries, the model is forced by a 1° resolution global solution of the MITgcm. Vertical mixing is parameterized by the nonlocal K-Profile Parameterization (KPP) scheme [*Large et al*., 1994]. The background coefficient of horizontal viscosity was set to 3×10^9 m^4 s^{-1} and background coefficients of vertical viscosity and diffusion were set to 1×10^{-4} and 1×10^{-5} m^2 s^{-1}, respectively.

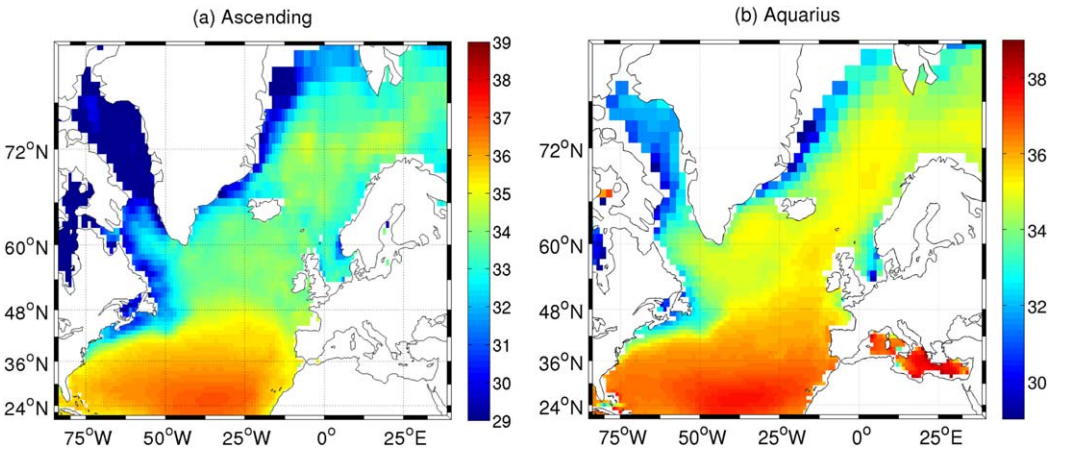

Figure 3. (a) Annually averaged SMOS SSS for the period from May 2012 to April 2013 from ascending arcs, after the elimination of a radio frequency interference source on Greenland. (b) Annually averaged Aquarius SSS for the same period.

During the course of this study, we use the daily averaged salinity output from the uppermost model level at 2.5 m depth, which henceforth will be referred to as model surface salinity.

3. Bias Estimate for SMOS Salinity Retrievals

A typical example of a SMOS SSS result is displayed in Figure 3a, showing the average SSS field for the period May 2012 to April 2013; the corresponding field based on Aquarius SSS data is shown in Figure 3b. Visible in both fields are the subtropical salinity maximum and the spread of high-salinity waters from the subtropics toward the subpolar North Atlantic and even into the Nordic Seas. Well represented in both data sets are also the low salinities along the Greenland and Icelandic coasts, which represent the advection of the low-salinity waters originating from the spring-summer sea-ice melting within the East Greenland Current, the latter also transporting polar waters from the Arctic Ocean into the Atlantic Ocean. In addition, the Aquarius SSS retrieval reveals the freshwater in the North Sea, which partially originates from the Baltic Sea (not resolved by SMOS).

A visual comparison of both fields reveals a smoother SMOS field. This is attributable to the gridding procedure as well as the singularity analysis fusion technique, during which the data were smoothed along the gradients. In addition, due to the wider swath and the smaller grid size in the used SMOS L4 product, more SMOS salinity values are averaged in $1^\circ \times 1^\circ$ grid cells during 1 month than for Aquarius, resulting in an enhanced noise compression in SMOS data over each grid cell. We also note that SMOS shows significantly lower salinity retrievals, especially in the eastern side of the basins and in a band from Iceland to Great Britain. Indeed, the main RFI source in the study area was switched off before May 2012 but with the switch off, weaker sources underneath turned more visible and still lead to an underestimation in the retrieved SSS values or data loss [*Daganzo-Eusebio et al*., 2013]. Averaged over the study area, the mean difference between both fields is -1.1 g/kg.

For a quantitative test of the quality of the satellite SSS retrievals, we computed the local standard deviation (STD) of all SMOS and Aquarius fields over the period May 2012 to April 2013 (including seasonal signals) and compared the resulting geographic variations of respective amplitudes with the model and in situ salinity (Figure 4). For SMOS, respective salinity fields were computed separately for ascending and descending tracks. The figure reveals that the geographic variability of both the Aquarius SSS STD and the ascending SMOS SSS STD are in good agreement with the model's uppermost salinity STD. In particular, both fields show high variability in frontal areas and in the Baffin Bay, Greenland and Barents Seas. Those high variabilities can also be found in the STD of the World Ocean Database salinity (WOD 2009) [*Seidov et al*., 2010], reaching amplitudes up to 1.2 g/kg, reflecting the irregular sampling and interannual variability. Spatial patterns of in situ STD are very similar to the model's uppermost salinity STD patterns, which motivated us to use model salinities in further analyses.

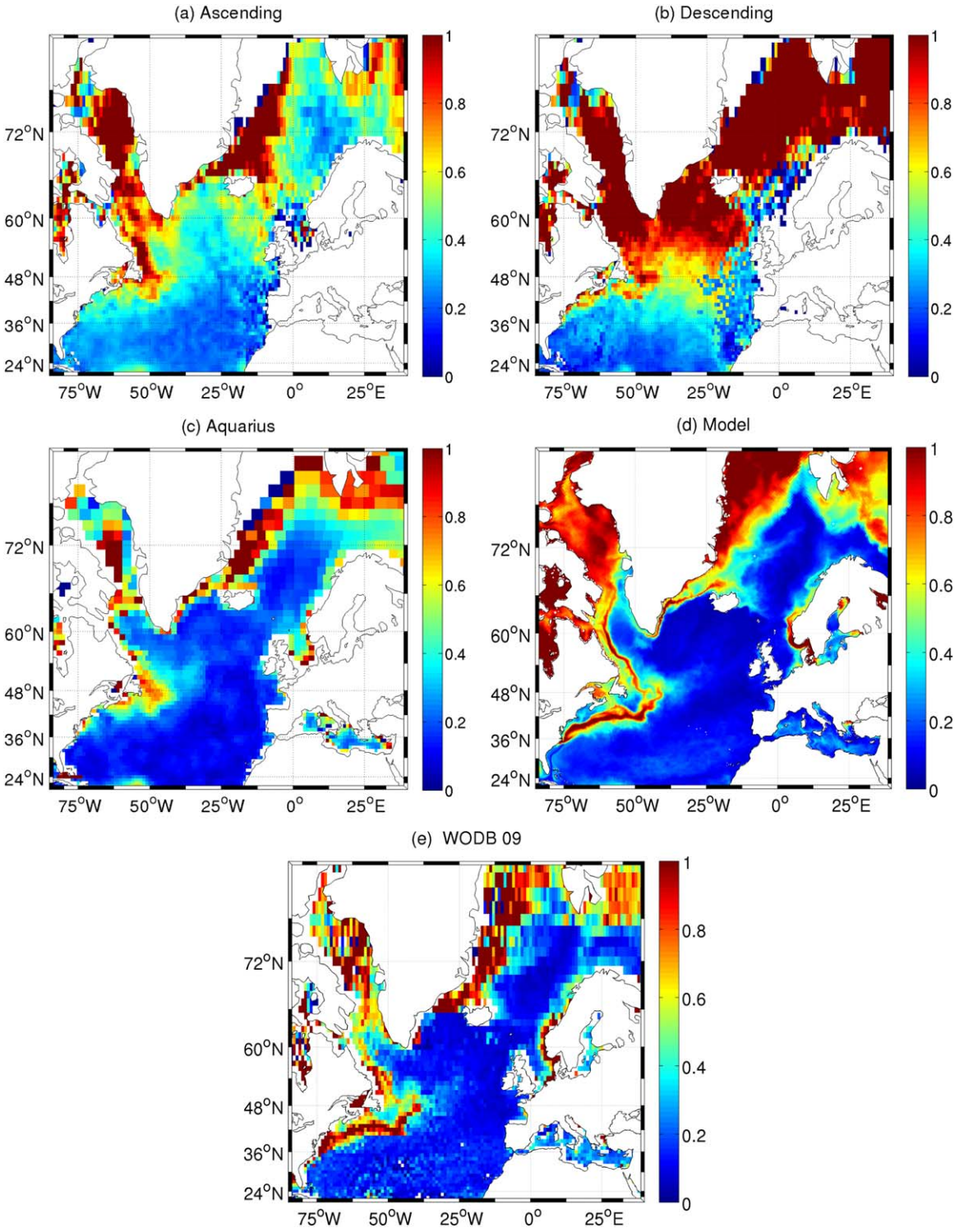

Figure 4. Standard deviation of salinity for the period from May 2012 to April 2013 from (a) SMOS ascending orbits, (b) SMOS descending orbits, and (c) Aquarius data. For comparison, (d) presents the respective results from the numerical ocean simulation (at 4 km resolution) in the period 2005–2009, and (e) the salinity standard deviation from the World Ocean Database 2009 [*Seidov et al.*, 2010].

In contrast to the other fields, descending SMOS arcs suggest unrealistically high SSS variability over the entire subpolar North Atlantic, reaching amplitudes of 2.7 g/kg. This is much larger than any of the other fields and higher than what could be expected from the model results. We therefore have to conclude that uncertainties in descending SMOS arcs are unrealistically high in the North Atlantic.

Averaged over the study area, the SMOS SSS variability from ascending orbits is ~0.5 g/kg; over the same area, the Aquarius SSS variability is ~0.3 g/kg. The SMOS field shows also high variability along the Greenland-Iceland-Scotland Ridge and over large parts of the Labrador Sea, which cannot be found in the Aquarius and in the model salinity standard deviations and probably reflects the influence of land contamination and the impact of above mentioned remaining RFI sources. Aquarius results agree somehow better with the model salinity variability structures than SMOS fields, especially in the Labrador Sea, close to Scandinavian coasts and over the Greenland-Iceland-Scotland Ridge.

The annual-mean difference of the SMOS SSS retrievals relative to the World Ocean Atlas (WOA09) monthly climatology [*Seidov et al*., 2010] amount to −1.1 and −1.2 g/kg for ascending and descending orbits, respectively (Figures 5a and 5c), pointing to a substantial negative bias in the SMOS retrieval relative to the climatology over our study area. The mean difference of SMOS SSS retrievals relative to the Argo fields is −1.1 and −1.5 g/kg for ascending and descending arcs, respectively (Figures 5b and 5d). In both cases, differences are not uniform in space, but instead show clear structures with larger differences (up to >2 g/kg) occurring in the vicinity of the cold East Greenland Current and over the Greenland-Iceland-Scotland Ridge. Differences are substantially smaller (less than −0.5 g/kg) in warm subtropical waters (between 25°N and 40°N), suggesting a clear temperature-dependent bias of the SMOS SSS.

As was expected, Aquarius SSS retrievals are less biased when compared with climatology and Argo data (Figures 5e and 5f), since an SST-dependent bias was already removed in the Aquarius SSS product used here [*Meissner et al*., 2014]. Accordingly, the mean difference over the study area and period of 0.06 g/kg relative to the climatology is clearly smaller than what is seen in the case of SMOS. Relative to Argo data, it amounts to −0.2 g/kg, suggesting that any bias was properly removed by the correction procedure. However, we also note that, relative to SMOS, Aquarius SSS retrievals are actually positively biased in warm subtropical waters as well as along the North Atlantic Current; in contrast, Aquarius SSS retrievals remain negatively biased close to the Greenland coast relative to the climatology and to Argo fields, suggesting that a small regionally dependent bias remains, which possibly could also be due to other error sources.

Boutin et al. [2014] mentioned that the theoretical error of SMOS SSS to first order depends on the number of brightness temperature data used for the retrieval and on SST. To quantify the dependence of the SMOS SSS bias on SST, we display in Figures 6a and 6b the SMOS minus Argo salinity differences, separately for ascending and descending orbits, as a function of SST in the region 20°N to 80°N and 85°W to 35°E. The SST data used in this analysis are an auxiliary product provided in the ECMWF-analyzed meteorological fields taken from the original Level 2 Ocean Salinity User Data Product (UDP). Data, as well as a product description, can be downloaded from https://earth.esa.int/web/guest/data-access/browse-data-products/-/article/level-2-ocean-salinity-6895. For our comparison, SST fields were compiled by box averaging the original SST values on a 1° × 1° grid.

Figure 6a demonstrates that for SST values exceeding 20°C, both the SMOS median bias and the spread of the differences tend to diminish for both arcs. In contrast, for water colder than 5°C, the SMOS ascending median bias reaches −1.8 g/kg. The SMOS descending median bias (Figure 6b) is even larger and reaches −5 g/kg or less in water colder than 10°C. At the same time, the spread of the differences increases substantially in the cold temperature range. This is especially true for the descending arc data. Based on these results and the ones previously shown in Figure 5, the L4 data from the descending SMOS arcs were not considered in further analyses.

For the ascending arcs, an SST-dependent SMOS SSS bias was inferred empirically by averaging the SMOS-Argo differences for each SST bin. The resulting median and its respective root-mean-square (RMS) error are shown by the red curve and vertical bars in Figure 6a, respectively. We note that for cold temperatures the median bias of SMOS descending arc SSS relative to climatological salinities is smaller than the median bias relative to Argo. In the case of the SMOS ascending arcs, the two curves are nearly equivalent. However, the RMS errors of SSS minus climatology are higher than the RMS errors of SSS minus Argo data. Therefore, we decided to use the SST-dependent bias from satellite SSS minus Argo differences for correcting the SMOS L4 products. In the remaining study, this bias was subtracted from the SMOS L4 product.

Also shown in Figure 6c are the salinity differences between Aquarius and Argo as a function of SST for the same region and period as before. The Aquarius bias seems not to be significantly different from zero and

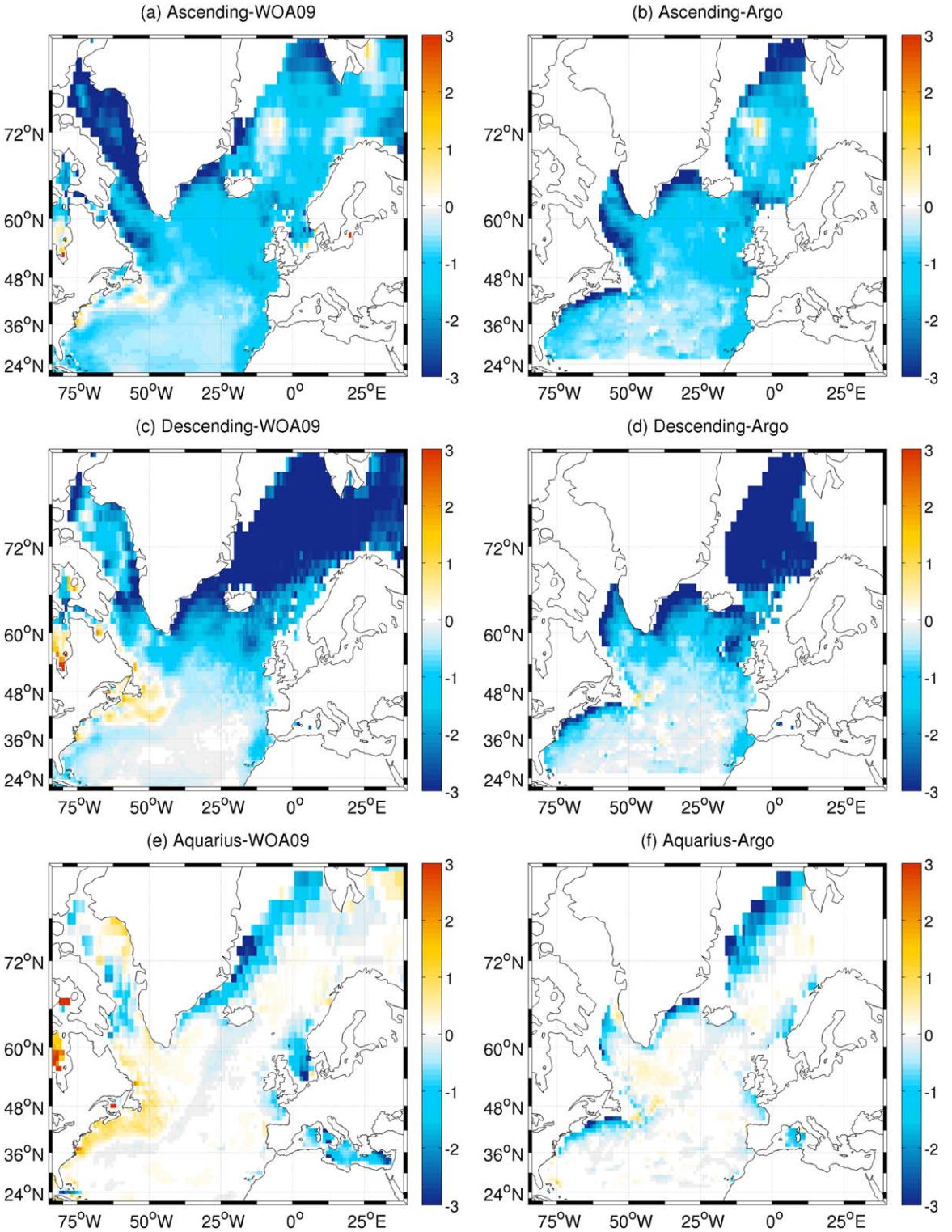

Figure 5. Average differences between (a) SMOS ascending SSS and the WOA09 surface salinity climatology, (b) SMOS ascending SSS and the Argo uppermost salinity, (c) SMOS descending SSS and the WOA09 surface salinity climatology, (d) SMOS descending SSS and the Argo uppermost salinity, (e) Aquarius SSS and the WOA09 surface salinity climatology, and (f) Aquarius SSS and the Argo uppermost salinity. All averages are for the period May 2012 to April 2013.

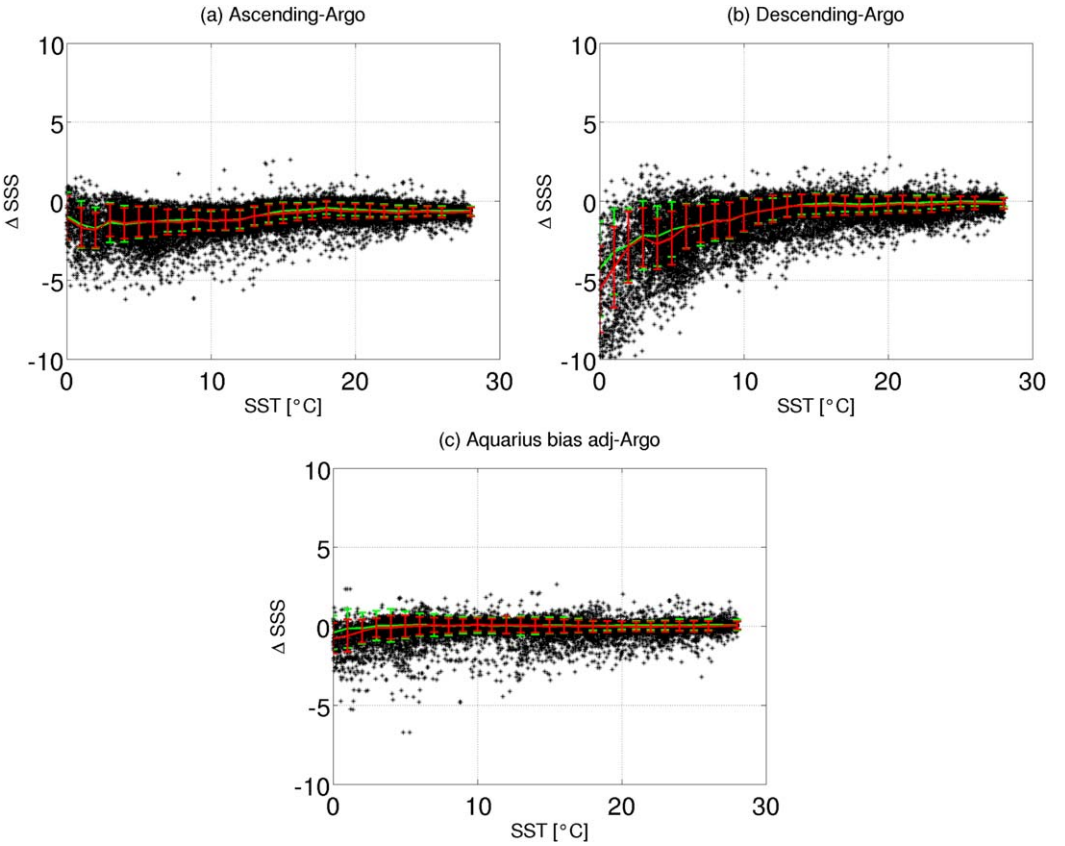

Figure 6. Difference between (a) SMOS ascending, (b) SMOS descending, and (c) Aquarius SSS retrievals for May 2012 till April 2013 and the Argo salinity for the same period, as a function of the ECMWF Sea Surface Temperature (SST) between 20°N and 80°N and 90°W and 15°E. A SST-dependent fit based on the median of the differences in 1°C temperature classes is overlaid in red, with the standard deviation of the salinity differences shown by the vertical bars. The SST-dependent fit based on the median of the differences to the WOA09 climatological salinities in 1°C temperature classes is overlaid in green, with the standard deviation of the salinity differences also shown by vertical bars.

slightly negative only below about 4°C. No bias correction was performed therefore in this study on top of what was already applied by the Aquarius project processing.

4. Processes Affecting the Satellite-In Situ Salinity Differences

Many factors can cause observed differences between satellite retrievals and in situ data and can especially lead to increased differences at lower temperatures visible in Figure 6. To some extent, those increased differences between SMOS and WOA09 fields can be attributed to a substantial undersampling of the climatological salinity data (i.e., an increased uncertainty in the WOA09 data) but also to the presence of interannual variability, which can be expected to be significant in this region of varying freshwater input due to sea ice or land ice melting. However, one also has to consider that some of the SMOS data were obtained in the vicinity of frontal structures, where temporal SSS variability is large (see Figure 4) and where therefore sampling errors are likely to occur. Associated processes can be linked to (i) temporal frontal and/or eddy-related variability and/or (ii) vertical near-surface salinity gradients.

In this context, one also has to take into consideration that monthly SMOS L4 SSS fields provided from the Barcelona Expert Centre are averages constructed by averaging data from 7 day repeats (only ascending arcs) on a 0.25° grid and which were smoothed in space by interpolating them onto a 1° by 1° spatial grid. On the other hand, in situ data represent instantaneous point-wise measurements sampled at just a few positions or only once along ship tracks (the case of TSG data used below) and averaged along track (nominally over 100 km segments). And because the average sampling rate of Argo floats is one sample every 10

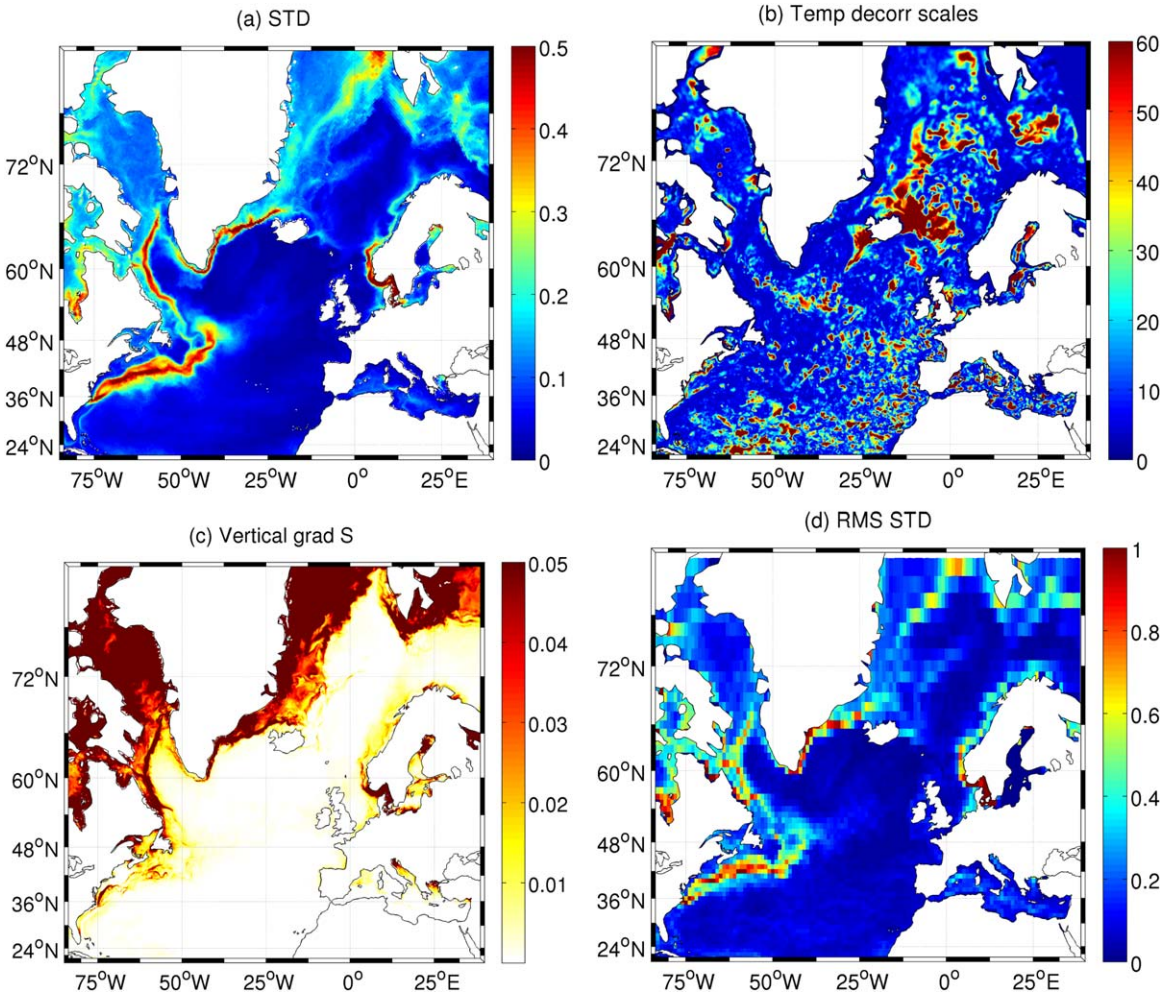

Figure 7. (a) Standard deviation of model uppermost salinity (with the seasonal cycle removed) on time scales smaller than 30 days. (b) Temporal decorrelation scales (units: days) computed from the model surface salinity (with the seasonal cycle removed). (c) Mean vertical salinity gradient (units: m^{-1}) inferred between 2.5 and 7.5 m depth from the same model. (d) Root-mean-square of all daily $1^\circ \times 1^\circ$ grid box standard deviations, which can be defined as a sampling root-mean-square error.

days nominally on a $3^\circ \times 3^\circ$ grid [*Tang et al.*, 2014] (in our study region, the sampling is substantially worse), that data set is not adequate to resolve small space-time scales of SSS variability. Consequently, the differences between satellite and in situ data shown can at least partially result from different spatial and temporal sampling of the strongly varying ocean SSS field, thereby leading to strong aliasing of SSS variability. In this sense, differences do not necessarily represent satellite data errors.

To quantify the potential impact of small-scale variability on the diagnosed salinity differences between SMOS and in situ measurements, we analyzed the standard deviation of the daily averaged near-surface (at 2.5 m depth) salinity field output from the model after high-pass filtering, thus retaining only fast salinity variations on time scales smaller than 30 days. As expected, high-frequency salinity variations are enhanced in the vicinity of frontal structures (e.g., north of the Gulf Stream axis) as well as close to the coast of Greenland, north of Iceland and within the East Greenland Current in the Irminger Sea (Figure 7a). Notably this also holds for the East Greenland Current, which suggests that the enhanced satellite-in situ differences diagnosed there could partially result from eddy processes being aliased in the nonsynchronously sampled observational data.

To determine how quickly the surface salinity field can change in a given time frame, we show in Figure 7b the temporal SSS decorrelation time scales computed as an *e*-folding decay time scale inferred from model salinity autocorrelation functions based on daily data (from which a time mean and a seasonal cycle were eliminated). The figure suggests that along the East Greenland Current salinity anomalies can decorrelate in

just a few days highlighting again the sampling problem one is facing in these regions. However, in the interior basin the decorrelation scales are substantially longer, approaching 30 days or more in some places and thereby making aliasing less problematic there. While this estimate might still be optimistic relative to the real world (because of a potential underrepresentation of fast processes in the model), it does give a useful estimate of what should be expected.

Since SMOS and Aquarius measurements are representative only for the top centimeter of the ocean, any vertical gradient of salinity in the upper few meters of the ocean can lead to a difference between satellite retrievals and Argo or ship-based observations usually taken at approximately 4 m depth or below. To quantify salinity differences arising from a vertical gradient in salinity in our study area, we estimated a near-surface salinity gradient from the numerical simulation using the model fields at 2.5 and 7.5 m depth (Figure 7c). Results suggest that in our study area vertical gradients over this depth range can be as large as 0.05 m^{-1}, with the largest vertical gradients residing close to the coast of Greenland and in the East Greenland Current frontal area. Assuming that gradients between the top centimeter of the ocean and 4 m depth are of the same order, these gradients could result in differences of up to 0.2 g/kg between satellite and in situ data.

Previously, *Boutin et al*. [2013] and *Henocq et al*. [2010] found that large vertical gradients in temperature and salinity can also exist due to precipitation events over the tropical oceans, leading to vertical salinity gradients over the upper 10 m of up to 0.5 g/kg [*Henocq et al*., 2010]. *Boutin et al*. [2014] studied the signature of rainfall with SMOS and drifter observations and found that, averaged over 1 month, the rain-induced surface salinity decrease is at most −0.2 g/kg and up to 40% of the difference between SMOS and interpolated in situ salinity near the ITCZ. However, due to the sparsity of simultaneous in situ measurements under rain events and SMOS data, *Boutin et al*. [2014] could not reach a conclusion about the vertical variability between the first cm of the water column and 4–5 m depth, where the uppermost Argo and TSG measurements originate. *Drucker and Riser* [2014] validated Aquarius L2 SSS against Argo salinities and analyzed the error due to the depth of measurements and vertical salinity stratification. They came to the conclusion, that insufficient collocation (horizontally and in the vertical) is not the most significant problem for the validation; instead they found that heavy rainfall can result in vertical differences as much as −1 g/kg (over the top 0–5 m). However, significant stratification events occurred only in <13% of their data (between 50°S and 50°N); therefore, the produced bias is much smaller than currently achievable L-band radiometric accuracies [*Drucker and Riser*, 2014]. Vertical salinity gradients diagnosed from the model fields tend to agree with those found in data from more equatorward areas, although they tend to be smaller. Nevertheless, we believe that vertical salinity gradients in most cases would not be a primary source of the difference diagnosed between SMOS or Aquarius and ship-based (or Argo) observations.

Regarding the aliasing of horizontal eddy-related SSS signals, *Vinogradova and Ponte* [2013] examined how much of a difference is expected between in situ salinity and Aquarius-derived salinity on the basis of their different sampling of spatial variability. To approximate the Aquarius footprint, daily salinity values from HYCOM were averaged by the authors onto a $1^\circ \times 1^\circ$ grid; the standard deviation within each box then represents the small-scale variability for every day of the year. Results indicate that in some pets of the ocean, small-scale variability can be an important source of sampling error for in situ measurements in regions of strong horizontal salinity gradients such as coastal areas, river outflows and along strong frontal structures, where a sampling error of up to 0.2 g/kg was diagnosed. From a similar computation but using our model output (Figure 7d), we can confirm the conclusion drawn by *Vinogradova and Ponte* [2013] but we find uncertainties which, with values of 1 g/kg, are substantially larger than those previously reported.

Besides processes in the ocean or biases of in situ data, a suite of remaining errors in satellite retrievals can also lead to differences relative to in situ data. As described in *Oliva et al*. [2013], the main error sources in SMOS measurements are antenna pattern, antenna loss, receiver, and correlation errors. The antenna pattern errors and side-lobes can cause spatial ripples. Of these, side-lobes are the dominant contributor to land-sea and ice-sea contamination, as well as sun and RFI tails spreading through the image (M. Martin-Neira et al., personal communication, 2013). The resulting increase of the signal again leads to an increase of the brightness temperature and therefore to lower SSS values [*Oliva et al*., 2012]. SSS retrievals around continents therefore have to be treated with caution and absolute salinity values are often erroneous. In addition, temporal drifts caused, e.g., by the strong influence of reflected solar radiation or by instrumental drifts due to the evolution of the antenna temperature within a year [*Kainulainen et al*., 2012] and short-term drifts [*Yin et al*., 2013], are also potential error sources.

5. Validation of Corrected Salinity Retrievals Against TSG Observations

In principle, all of the above mentioned error sources need to be considered when interpreting satellite-in situ SSS differences. However, many of the above biases show some correction with geographically changing temperature fields, their influence apparently can be reduced by removing an SST-dependent bias from the SMOS data. How good the resulting bias-corrected data are is the question addressed in what follows.

For a quality assessment of the bias-corrected SMOS SSS retrievals, Figure 8a shows the differences between the SMOS and Aquarius fields and the independent in situ TSG salinity observations. The figures compare monthly mean salinity fields from the satellites with the instantaneous in situ data averaged during the corresponding month on the same grid. In this context, the size of the shown circles corresponds to the number of data pairs available in the period from May 2012 to April 2013. Large remaining differences occur in the East Greenland Current region and along the Labrador Sea rim current, where the SMOS differences show negative and positive differences of roughly equal amplitude and on spatial eddy scales as they could be expected from eddy aliasing. Since similar differences result also from the Aquarius fields (Figure 8c), such a conclusion seems plausible. Further to the east, biases in both data sets tend to diminish. Individual fluctuations of ± 0.5 g/kg could be attributed to the above mentioned spatial ripples caused by land-sea, ice-sea and remaining RFI contamination.

Consistent with previous findings, areas of high-salinity differences between TSG and SMOS and Aquarius, respectively, correspond to areas of short decorrelation time scales, suggesting that at least some of those differences might result from aliasing of eddy SSS signal in the TSG data. High differences and short decorrelation time scales can be found for example in the East Greenland Current, Labrador Sea rim as well as south of Spitsbergen (Figure 7b). However, we also note that close to the Greenland coast it is very difficult to isolate the aliasing influence from other influences such as land contaminations. Nevertheless, the fact that both difference fields are fairly similar suggest that remaining data issues present in SMOS and Aquarius data seem to have been corrected in quite the same efficient way through the SST-related bias correction.

Histograms of SMOS-TSG differences, shown in Figure 8b, characterize the remaining bias (red bars), but also the remaining uncertainty in the data. Also included in the figure are SSS errors prior to the bias correction (blue bars), illustrating a shift of the peak in the histograms toward a zero mean. As can be seen from the figure, the bias correction was able to remove an offset in this region. The SMOS bias could thus be reduced from -1.2 up to 0.1 g/kg and the RMS error is reduced from 1.5 g/kg prior to and 0.9 g/kg after the bias correction; but the standard deviation of the differences remains high with 0.9 g/kg (before and after the bias correction). The statistics of SMOS SSS minus TSG salinities before and after bias correction are summarized in Table 1.

The mode of the histogram of the Aquarius V3 $SSS_{bias-adj}$ minus TSG differences (Figure 8d, red) is almost zero (mean difference is 0.02 g/kg), but the RMS error is, with 0.9 g/kg, very similar to the SMOS RMS value. For a comparison, the earlier version (V2.0) of the Aquarius Level 3 data (shown in blue), which was not SST bias corrected (ftp://podaac-ftp.jpl.nasa.gov/allData/aquarius/docs/v3/Aquarius_V2_V3_Comparisons.norman_kuring.2june2014.pdf), shows a bias up to -3 g/kg in cold waters, which tends to diminish for waters warmer than 8°C. Here, the median bias reaches -0.5 g/kg in cold waters, which also could be attributable to other error sources like land-sea contamination. The STD of the differences reduces from 1.6 to 0.9 g/kg between Aquarius V2 and V3 (compare Table 1), illustrating again the efficiency of the SST bias correction.

Since we compare monthly gridded TSG and satellite values we cannot estimate monthly standard deviations. To investigate how representative monthly averaged gridded TSG data are of the total monthly salinity average within one grid box, we resampled the model daily averaged salinities at the TSG positions and gridded them on the same spatial and temporal grid and compared these with the total gridded model salinity field (Figure 8e). Areas with high mean differences imply that there the gridded TSG values did not capture the total SSS. As shown, differences are higher than 0.5 g/kg close to the Scandinavian coast and again in frontal regions in the western part of the study area. The root-mean-square over all differences is 0.38 g/kg, with the highest values in coastal and variable areas. There, the validation results have to be taken with caution. That is, large differences between satellite and in situ data could be attributed to sampling errors in the TSG measurements. However, more in situ data are needed to quantify this exactly. It could be helpful to consider the differences of individual measurements rather than gridded values [*Boutin*

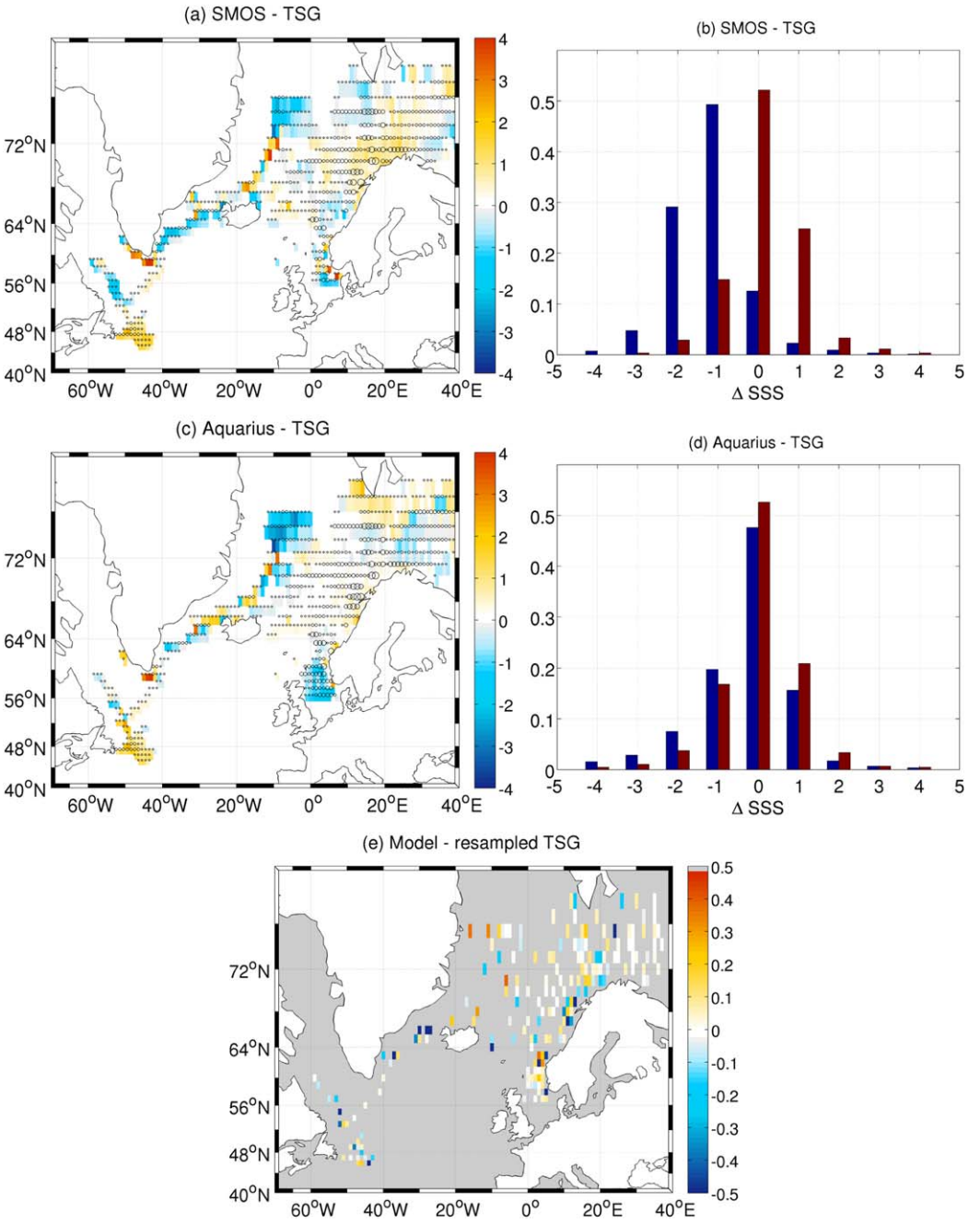

Figure 8. Mean differences between 1° gridded satellite-derived salinity and 1° gridded in situ TSG salinity for the 1 year period from May 2012 to April 2013 (excluding January 2013): (a) using the bias-corrected SMOS SSS ascending orbits, and (c) using the Aquarius SSS. Dots correspond to one data pair and the largest circles to 11 pairs. (b) Histograms of mean differences between 1° gridded SMOS SSS ascending orbits and 1° gridded TSG salinities before (blue) and after (red) the bias correction was applied. (d) Histograms of mean differences between 1° gridded Aquarius V2 SSS (blue) and Aquarius V3 bias adjusted SSS (red) and 1° gridded TSG salinities. (e) Mean differences between 1° gridded model salinity and 1° gridded model salinity resampled at the TSG locations.

et al., 2013; *Vinogradova and Ponte*, 2013]. But in this case, it is difficult to find SMOS or Aquarius SSS and in situ samples collocated within short time and spatial scales in the study area and period.

6. Annual Cycle of Monthly Salinity Anomalies

The amplitude of the annual cycle of salinity was calculated by M. Sena Martins et al. (Spatial and temporal scales of sea surface salinity variability in the Atlantic Ocean, submitted to *Journal of Geophysical Research*,

Table 1. Statistics of Satellite-Retrieved SSS Minus TSG Salinities Before and After Bias Correction

Data Product	Mean	STD	RMSE	R
SMOS L4	−1.2	0.9	1.5	0.6
SMOS $L4_{bias-corr}$	0.1	0.9	0.9	0.6
Aquarius V2	−0.5	1.6	1.7	0.4
Aquarius V3 $SSS_{bias-adj}$	0.02	0.9	0.9	0.6

2014) from the same 4 km resolution model output as well as from gridded in situ data. The amplitude is largest (>1 g/kg) in the rim of the Baffin Bay, Labrador Sea, and Greenland Sea. Changes in sea-ice coverage and associated brine rejection during ice formation have a direct effect on SSS in these areas; an increased amplitude of the annual cycle along the rims of the Labrador Sea and in the Greenland Sea is caused by the advection of water from ice-covered areas [*Boyer and Levitus*, 2002]. The annual signal reaches large (>1 g/kg) values along the East and West Greenland Currents as well as along the rim of the Labrador Sea. A high-amplitude seasonal cycle can also be found off the Scandinavian coast, in the areas of Baltic Sea outflow, and in the North Sea due to freshwater runoff. The phase (year day of maximum SSS) of the annual cycle is centered in fall and winter in the East Greenland Current and Labrador Sea's rim. Because satellite data are still subject to seasonally varying biases, they are not yet qualified for a quantitative estimate of the seasonal cycle.

To demonstrate the benefit SMOS SSS fields might provide even for studies of salinity variability in the subpolar Atlantic, we present in Figure 9 selected monthly salinity anomalies (relative to the annual mean) and compare them to salinity anomalies derived from the eddy-resolving simulation and Argo floats. Shown are monthly SMOS SSS anomalies for May, August, October, and January between May 2012 and April 2013, after correcting the fields for the SST-dependent bias, and monthly Aquarius anomalies for corresponding months and study period. Whereas, the satellite retrieved salinities, as well as the Argo salinity fields, are from 2012 to 2013, the model fields are from 2005 to 2006. There are interannual changes in the salinity anomaly fields due to a different amount of ice melting in different years, which regionally reach up to 0.5 g/kg along the northern ice edges in winter, in the eastern rim of the East Greenland Current during summer months and along the North Atlantic Current axis (not shown). However, we chose the 2005–2006 period because a simultaneous model output is not available but the chosen period compares quite well to the fields of 2012 and 2013 Argo salinity anomalies and helps to interpret those in situ fields. The substantially degraded spatial resolution in the Argo fields underlines, in an impressive way, the large potential the satellite SSS data can play in describing monthly salinity variations with much improved spatial details.

Starting in May, the model shows high-salinity anomalies below the sea-ice due to brine release during the freezing period. We find fresh anomalies at the ice edge in the Nordic Seas and along the East Greenland Current, continuing around the Labrador Sea into the Labrador Current. In general, the North Atlantic region shows positive anomalies north of 40°N but negative anomalies in the eastern subtropics. The SMOS field captures the positive anomalies and the fresh anomalies along the northeastern rims, however, there seems to be a positive anomaly in the whole field of May. The Aquarius SSS compares well with that from SMOS, except along the Norwegian coast and around Great Britain, where Aquarius positive anomalies tend to agree with the model.

In August, negative model anomalies reflect the advection of the freshwater input during the melting season in the whole western North Atlantic. In the western subtropics, the fresh anomalies can be associated to other processes like advection from the south [*Yu*, 2011], and in the eastern subtropics positive anomalies indicate the summer salinity maximum forced, as explained in *Qu et al.* [2011], by horizontal advection and vertical entrainment. Both satellite-retrieved salinity fields show the negative anomalies in the Greenland Sea, the Iceland Sea, the Labrador Sea, and the region of the Gulf Stream/North Atlantic Current; furthermore, both products show the positive salinity anomalies in the eastern subtropics. The main difference between SMOS and Aquarius resides over the eastern part of the Greenland-Scotland-Iceland Ridge, where Aquarius shows positive anomalies and SMOS negative anomalies. The latter is, in this case, in closer agreement with the model.

In October, positive model anomalies, in the beginning of the freezing season, can be found at the ice edge due to processes like brine release (they are possible to be shown for the model fields, but not for the satellite fields). The in situ data also show positive anomalies in the western part of the Greenland Sea. Negative anomalies still dominate in the western part of the North Atlantic and positive values are seen in the southeastern Atlantic. Turning to the SMOS salinity anomalies, the start of the freezing season can be encountered as well and also slightly positive anomalies in the eastern subtropics are shown. However, the October field is negative in the remaining domain. In October, the Aquarius salinity anomalies agree

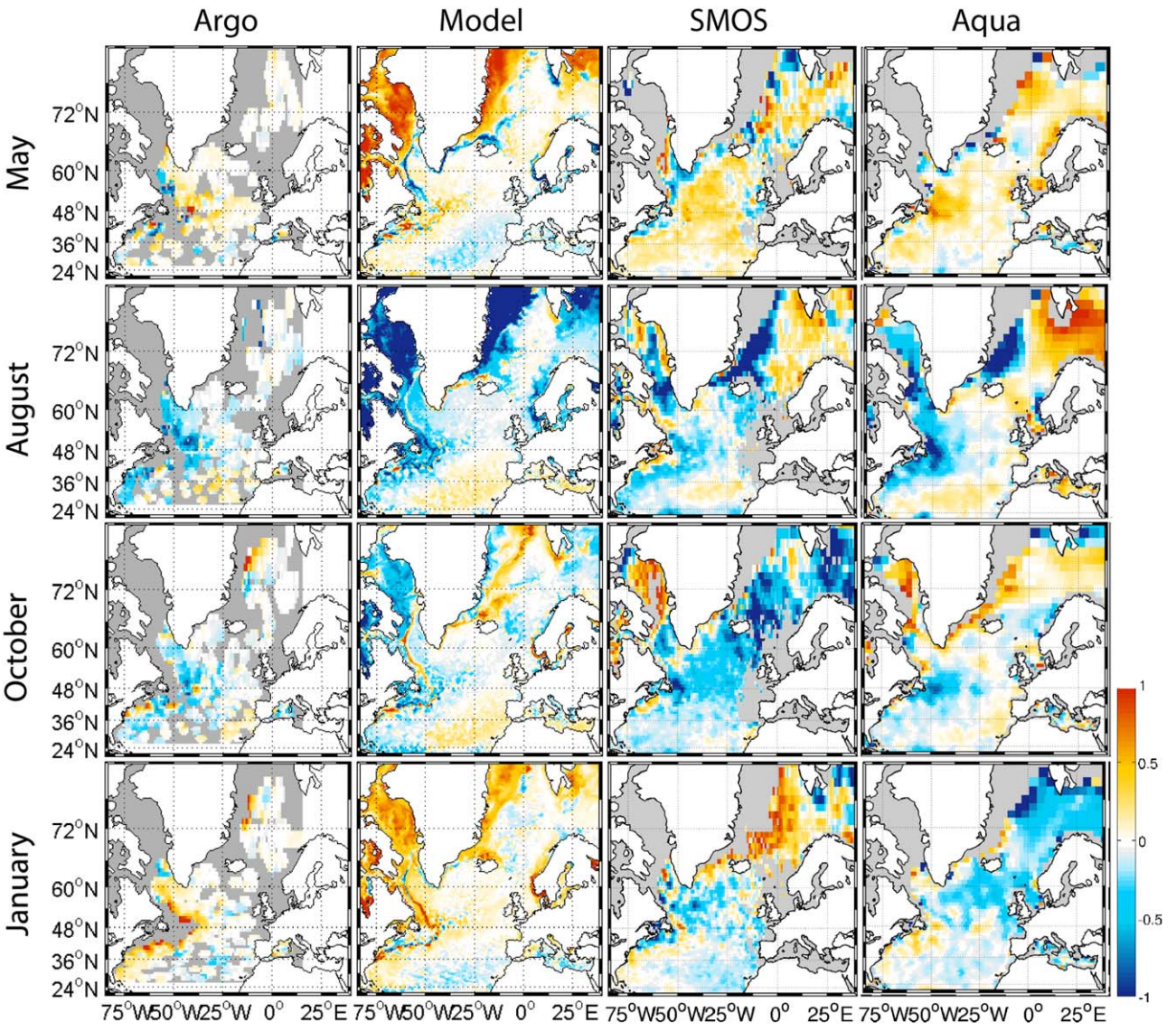

Figure 9. Monthly salinity anomalies (relative to the annual mean) from (first column) the Argo floats, (second column) the 4 km resolution model, (third column) the 1° gridded and bias-corrected SMOS ascending SSS, and (fourth column) the 1° gridded Aquarius SSS. Shown are the months of May, August, and October in 2012 and January in 2013 (2005 and 2006 in the model case). Negative anomalies up to −1 are shown in blue, positive anomalies up to 1 in red. Color scale is saturated. Dark gray shading indicates no data.

reasonably well with the model and Argo anomalies. But in this case, the Barents Sea's Aquarius anomalies are positive, whereas the model and SMOS point to negative anomalies there.

The January salinity anomalies show an opposite picture of the August field, with positive model anomalies in the freezing season under the ice due to brine release. Also the salinity anomalies are positive at the ice edge as well as along the western rim of the study region around the Grand Banks of Newfoundland. The negative phase of the annual cycle of salinity can be found in the subtropics, in accordance to the Argo salinity anomaly field. Whereas both SMOS and Aquarius contain the negative anomalies in the eastern subtropics and agree off the Gand Banks, the salinities are quite different in the Nordic Seas, where SMOS tends to agree with the model results but Aquarius shows a negative widespread anomaly.

7. Concluding Remarks

We have shown in this study that, relative to ship-based in situ near-surface salinity measurements, the SMOS and Aquarius SSS fields show realistic spatial and temporal variations of the surface salinity field during the

period May 2012 to April 2013 which is analyzed here. Overall, the L4 SMOS salinities are lower than climatological and in situ salinity, especially in cold water regions. The bias can be improved through an SST-dependent bias correction inferred empirically as a (in space and time) relation between satellite and Argo data in the North Atlantic (>20°N). Regarding the SMOS L4 SSS descending arc data, they appear substantially corrupted in the North Atlantic and were not considered in the later analyses of this study. After the removal of the SST-dependent bias, the offset between SMOS SSS and independent TSG salinity observations taken in the Nordic Seas and subpolar North Atlantic is substantially reduced. However, the spread of differences between satellite and in situ data in colder waters remains high. Using longer time series, we believe, however, that results can be further improved.

Aquarius overestimates SSS in warm subtropical waters as well as along the North Atlantic Current in comparison to climatology and in situ observations; but the biases are more than 1 g/kg smaller than for the SMOS fields since it was previously already corrected through an SST-dependent bias correction. After applying a bias correction to SMOS, one can start finding agreements between satellite SSS retrievals and in situ fields. Our method of the bias correction applied to the L4 SMOS data is confirmed by the similar comparison between Aquarius and independent TSG observations. In both cases, correlation coefficients of 0.6 between in situ TSG salinity anomalies with SMOS and Aquarius were found.

In an overall sense, our study suggests that even in cold waters the satellite SSS retrievals show skill in observing changes of the ocean surface salinity. With an equivalently improved retrieval algorithm that remedies the fresh SMOS SSS bias in cold waters, with the elimination of lingering land contamination in the SMOS SSS field, and with longer time series of data from SMOS and Aquarius, we will be able to study changes in salinity over all parts of the world ocean and to start constraining ocean models by satellite SSS data in combination with Argo subsurface salinity observations, so as to better compute transports of freshwater as well as surface freshwater fluxes between the ocean and the atmosphere. Satellite-based SSS observations need to be part of our sustained long-term climate observing system. Despite the unprecedented in situ Argo salinity sampling, spatial structures remain poorly resolved spatially in contrast to the satellite retrievals.

Before a full use of SMOS and Aquarius fields can be made for quantitative studies of salinity variations and underlying causes, an improved uncertainty description of the data and ultimately an improved data quality is needed. Until then, analyzing satellite salinity retrievals in high latitudes remains a challenge. In particular, our study shows that the quality of the SMOS L4 SSS fields remains preliminary in the subpolar areas. At least there, the retrieval algorithm remains highly sensitive to a number of environmental and instrumental factors contributing to remaining uncertainties in the retrievals.

In reality, SMOS SSS retrievals in high northern latitudes are still plagued by a suite of remaining errors like RFI contamination from remaining sources, land-sea and ice-sea contamination and the reduced sensitivity of the brightness temperature to salinity variations in cold waters. A quantitative study of potential errors in this region remains a problematic task since isolating each type of bias is difficult. In some of those regions, local differences between satellite salinities and in situ salinities, particularly in regions of large freshwater input like the Greenland shelf, actually have to be attributed, at least partly, to temporal variability of the position of the local salinity front. *Köhl et al.* [2014] present an alternative approach to infer biases in satellite SSS retrievals using a dynamically consistent assimilation methodology.

Different SMOS SSS products have been developed by several institutions and similar analyses using other SMOS products (not shown) lead to different results, attributable to different strategies for correcting the errors. *Zhang et al.* [2013] compared two SMOS products (BEC L3 and CATDS V02) with Argo measurements and showed that both products perform well in the open low-latitude oceans; but close to coasts and in higher latitudes the biases were high. The reasons for using the BEC L4 product in the present study are, on the one hand, the availability of data in the study period and, on the other hand, that frontal structures are potentially better taken into account, which is of special importance in our study area. However, our results suggest that more work needs to be done along those lines.

We used a model simulation to gain insight into realistic levels of salinity variability, on the impact of oceanographic processes in the latter and to deduce sampling errors in the observations. The quality of the model estimates, however, are affected by forcing errors from the atmospheric reanalysis, by the lack of high-frequency forcing, the lack of resolution for certain subgrid-scale processes, and the imperfection of their parameterizations and by natural ocean internal variability.

In closing, we note that more studies like the one presented here are required to determine the quality of the satellite SSS data over all parts of the global ocean and to help improving the inversion algorithms. A problem for further improving satellite SSS retrievals in high latitudes is the lack of in situ measurements there required for validation and correction of the satellite retrievals. To what extent a sampling error affects the validation results is an important point for further studies. Our results are based only on a study period of 1 year; the analysis of a multiyear period and more in situ measurements in the higher northern latitudes would be helpful to test the robustness of our validation results. In the best case, one would be tempted to use only single satellite-based samples as well as individual in situ samples in order to minimize collocation errors, but it is difficult to find SMOS or Aquarius SSS and in situ samples collocated within short time and spatial scales. Therefore an up-to-date, global, uniform, quality-checked data base of in situ measurements, especially TSG sections, would be an asset.

Acknowledgments

We thank Detlef Quadfasel (Institut für Meereskunde, Universität Hamburg) and Katrin Latarius (Alfred Wegener Institut für Polarforschung, Bremerhaven), Allan Cembella (Alfred Wegener Institut für Polarforschung, Bremerhaven), Dagmar Kieke (Institut für Umweltphysik, Bremen), and Johannes Karstensen (GEOMAR Helmholtz Centre for Ocean Research, Kiel) for providing the thermosalinograph data obtained during cruises of the German R/V "Poseidon" and R/V "Maria S. Merian." We also wish to thank the Norwegian Marine Data Centre (NMD) at the Institute of Marine Research, Norway, for providing TSG measurements from aboard of the Norwegian R/V "Johan Hjort" and R/V "G.O. Sars." Argo data were collected and made freely available by the International Argo Project and the national initiatives which contribute to it (http://www.argo.net). The Aquarius satellite SSS data were supplied through the NASA/CONAE Aquarius/SAC-D Project and can be downloaded from http://podaac.jpl.nasa.gov. At the time of the study, the SMOS SSS L4 product was available at http://cp34-bec.cmima.csic.es/ocean-reprocessed-dataset. These data were produced by the Barcelona Expert Center (http://www.smos-bec.icm.csic.es), a joint initiative of the Spanish Research Council (CSIC), and the Technical University of Catalonia (UPC), mainly funded by the Spanish National Program on Space. We thank Meike Demgen for the assistance in the figure preparation. We also thank the anonymous reviewers, who helped improving the manuscript. This work has been supported in part through German SMOS CAL/VAL activities funded by the BMBF through contract 50EE1245 and in part through the DFG funded Forschergruppe FOR1740. Julia Köhler acknowledges a scholarship from the Max-Planck Research School for Maritime Affairs. The numerical simulation was conducted at the German Climate Computing Center (DKRZ), Hamburg, Germany, in the frame of project 704. This work is a contribution to the DFG funded Excellence Initiative CliSAP at the University of Hamburg.

References

Banks, C., C. Gommenginger, M. Srokosz, and H. Snaith (2012), Validating SMOS ocean surface salinity in the Atlantic with Argo and operational ocean model data, *IEEE Trans. Geosci. Remote Sens.*, *50*(5), 1688–1702, doi:10.1109/TGRS.2011.2167340.

Boutin, J., N. Martin, G. Reverdin, X. Yin, and F. Gaillard (2013), Sea surface freshening inferred from SMOS and ARGO salinity: Impact of rain, *Ocean Sci.*, *9*(1), 183–192, doi:10.5194/os-9-183-2013.

Boutin, J., N. Martin, G. Reverdin, S. Morisset, X. Yin, L. Centurioni, and N. Reul (2014), Sea surface salinity under rain cells: SMOS satellite and in situ drifters observations, *J. Geophys. Res. Oceans*, *119*, 5533–5545, doi:10.1002/2014JC010070.

Boyer, T. P., and S. Levitus (2002), Harmonic analysis of climatological sea surface salinity, *J. Geophys. Res.*, *107*(C12), 8006, doi:10.1029/2001JC000829.

Daganzo-Eusebio, E., R. Oliva, Y. H. Kerr, S. Nieto, P. Richaume, and S. Mecklenburg (2013), SMOS radiometer in the 1400–1427-MHz passive band: Impact of the RFI environment and approach to its mitigation and cancellation, *IEEE Trans. Geosci. Remote Sens.*, *51*(10), 4999–5007.

Dee, D. P., et al. (2011), The ERA-Interim reanalysis: Configuration and performance of the data assimilation system, *Q. J. R. Meteorol. Soc.*, *137*(656), 553–597, doi:10.1002/qj.828.

Donlon, C. J., M. Martin, J. Stark, J. Roberts-Jones, E. Fiedler, and W. Wimmer (2012), The operational sea surface temperature and sea ice analysis (OSTIA) system, *Remote Sens. Environ.*, *116*, 140–158, doi:10.1016/j.rse.2010.10.017.

Drucker, R., and S. C. Riser (2014), Validation of Aquarius sea surface salinity with Argo: Analysis of error due to depth of measurement and vertical salinity stratification, *J. Geophys. Res. Oceans*, *119*, 4626–4637, doi:10.1002/2014JC010045.

Durack, P. J., and S. E. Wijffels (2010), Fifty-year trends in global ocean salinities and their relationship to broad-scale warming, *J. Clim.*, *23*, 4342–4362, doi:10.1175/2010JCLI3377.1.

ESA (2012), SMOS satellite measurements improve as ground radars switch off [online]. [Available at http://www.esa.int/Our_Activities/Observing_the_Earth/SMOS_satellite_me asurements_improve_as_ground_radars_switch_off.].

Font, J., G. S. E. Lagerloef, D. L. Vine, A. Camps, and O. Zanife (2004), The determination of surface salinity with the European SMOS Space Mission, *IEEE Trans. Geosci. Remote Sens.*, *42*, 2196–2205.

Font, J., et al. (2013), SMOS first data analysis for sea surface salinity determination, *Int. J. Remote Sens.*, *34*(9–10), 3654–3670, doi:10.1080/01431161.2012.716541.

Gabarro, C., M. Portabella, M. Talone, and J. Font (2009), Toward an optimal SMOS ocean salinity inversion algorithm, *IEEE Geosci. Remote Sens. Lett.*, *6*(3), 509–513, doi:10.1109/LGRS.2009.2018490.

Gabarro, C., J. Martinez, and J. Font (2012), Impact of the land-sea contamination on SMOS retrieved salinity, *Tech. Rep. 1.0*, SMOS Barcelona Expert Centre, Institute of Marine Sciences, Barcelona, Spain.

Guimbard, S., J. Gourrion, M. Portabella, A. Turiel, C. Gabarro, and J. Font (2012), SMOS semi-empirical ocean forward model adjustment, *IEEE Trans. Geosci. Remote Sens.*, *50*(5), 1676–1687, doi:10.1109/TGRS.2012.2188410.

Helm, K. P., N. L. Bindoff, and J. A. Church (2010), Changes in the global hydrological-cycle inferred from ocean salinity, *Geophys. Res. Lett.*, *37*, L18701, doi:10.1029/2010GL044222.

Henocq, C., J. Boutin, F. Petitcolin, G. Reverdin, S. Arnault, and P. Lattes (2010), Vertical variability of near-surface salinity in the tropics: Consequences for L-Band radiometer calibration and validation, *J. Atmos. Oceanic Technol.*, *27*, 192–203.

Hosoda, S., T. Suga, N. Shikama, and K. Mizuno (2009), Global surface layer salinity change detected by Argo and its implication for hydrological cycle intensification, *J. Oceanogr.*, *65*, 579–586.

Jacobs, S. S., and C. F. Giulivi (2010), Large multidecadal salinity trends near the Pacific-Antarctic continental margin, *J. Clim.*, *23*, 4508–14,524, doi:10.1175/2010JCLI3284.1.

Kainulainen, J., A. Colliander, J. Closa, M. Martin-Neira, R. Oliva, G. Buenadicha, P. Rubiales Alcaine, A. Hakkarainen, and M. T. Hallikainen (2012), Radiometric performance of the SMOS reference radiometers—Assessment after one year of operation, *IEEE Trans. Geosci. Remote Sens.*, *50*(5), 1367–1383.

Kim, S., J. H. Lee, P. de Matthaeis, S. Yueh, C.-S. Hong, J.-H. Lee, and G. Lagerloef (2014), Sea surface salinity variability in the east china sea observed by the Aquarius instrument, *J. Geophys. Res. Oceans*, *119*, 7016–7028, doi:10.1002/2014JC009983.

Köhl, A., M. Sena Martins, and D. Stammer (2014), Impact of assimilating surface salinity from SMOS on ocean circulation estimates, *J. Geophys. Res. Oceans*, *119*, 5449–5464, doi:10.1002/2014JC010040.

Lagerloef, G., et al. (2008), The Aquarius/SAC-D Mission: Designed to meet the salinity remote-sensing challenge, *Oceanography*, *21*(1), 68–81.

Large, W. G., J. C. McWilliams, and S. C. Doney (1994), Oceanic vertical mixing: A review and a model with nonlocal boundary layer parameterization, *Rev. Geophys.*, *32*, 363–403.

Lee, T., G. S. E. Lagerloef, M. M. Gierach, H. Kao, S. Yueh, and K. Dohan (2012), Aquarius reveals salinity structure of tropical instability waves, *Geophys. Res. Lett.*, *39*, L12610, doi:10.1029/2012GL052232.

Marshall, J., A. Adcroft, C. Hill, L. Perelman, and C. Heisey (1997b), A finite-volume, incompressible Navier Stokes model for studies of the ocean on parallel computers, *J. Geophys. Res.*, *102*, 5753–5766.

Martinez, J. (2013), Ocean RFI distribution, *Tech. Rep. 1.0*, SMOS Barcelona Expert Centre, Institute of Marine Sciences, Barcelona, Spain.

McMullan, K. D., M. Brown, M. Martin-Neira, W. Rits, S. Ekholm, J. Marti, and J. Lemanczyk (2008), SMOS: The payload, *IEEE Trans. Geosci. Remote Sens.*, *46*(3), 594–605, doi:10.1109/TGRS.2007.914809.

Meissner, T., F. Wentz, D. L. Vine, and J. Scott (2014), Addendum III to ATBD, technical report Nr. 060414, Remote Sensing Systems, Santa Rosa, Calif.
Morisset, S., et al. (2012), Surface salinity drifters for SMOS validation, *Mercator Ocean—CORIOLIS Quart. Newslett.*, *45*, 33–37.
Oliva, R., E. Daganzo, Y. Kerr, S. Mecklenburg, S. Nieto, P. Richaume, and C. Gruhier (2012), SMOS radio frequency interference scenario: Status and actions taken to improve the RFI environment in the 1400 #x2013;1427-mhz passive band, *IEEE Trans. Geosci. Remote Sens.*, *50*(5), 1427–1439, doi:10.1109/TGRS.2012.2182775.
Oliva, R., M. Martin-Neira, I. Corbella, F. Torres, J. Kainulainen, J. Tenerelli, F. Cabot, and F. Martin-Porqueras (2013), SMOS calibration and instrument performance after one year in orbit, *IEEE Trans. Geosci. Remote Sens.*, *51*(1), 654–670, doi:10.1109/TGRS.2012.2198827.
Polyakov, I. V., V. A. Alexeev, G. I. Belchansky, I. A. Dmitrenko, V. V. Ivanov, S. A. Kirillov, A. A. Korablev, M. Steele, L. A. Timokhov, and I. Yashayaev (2008), Arctic Ocean freshwater changes over the past 100 years and their causes, *J. Clim.*, *21*(2), 364–384.
Qu, T., S. Gao, and I. Fukomori (2011), What governs the North Atlantic salinity maximum in a global GCM, *Geophys. Res. Lett.*, *38*, L07602, doi:10.1029/2011GL046757.
Reul, N., et al. (2013), Sea surface salinity observations from space with the SMOS satellite: A new means to monitor the marine branch of the water cycle, *Surv. Geophys.*, *35*, 681–722, doi:10.1007/s10712-013-9244-0.
Seidov, D., T. P. Boyer, R. A. Locarnini, A. V. Mishonov, and H. E. Garcia (2010), *World Ocean Atlas 2009*, Volume 2, Salinity, NOAA Atlas NESDIS 69, 184 pp., U.S. Gov. Print. Off., Washington, D. C.
Serra, N., R. H. Käse, A. Köhl, D. Stammer, and D. Quadfasel (2010), On the low-frequency phase relation between the Denmark Strait and the Faroe-Bank Channel overflows, *Tellus, Ser. A*, *62*(4), 530–550, doi:10.1111/j.1600-0870.2010.00445.x.
SMOS-BEC Team (2014), SMOS-BEC ocean and land products description, *Tech. Rep. 1.2*, SMOS Barcelona Expert Centre, Institute of Marine Sciences, Barcelona, Spain.
Steele, M., R. Morley, and W. Ermold (2001), Phc: A global ocean hydrography with a high quality arctic ocean, *J. Clim.*, *14*, 2079–2087.
Tang, W., S. H. Yueh, A. G. Fore, and A. Hayashi (2014), Validation of Aquarius sea surface salinity with in situ measurements from argo floats and moored buoys, *J. Geophys. Res. Oceans*, *119*, 6171–6189, doi:10.1002/2014JC010101.
Turiel, A., V. Nieves, E. Garcia-Ladona, J. Font, M.-H. Rio, and G. Larnicol (2009), The multifractal structure of satellite sea surface temperature maps can be used to obtain global maps of streamlines, *Ocean Sci.*, *5*, 447–460.
Umbert, M., N. Hoareau, A. Turiel, and J. Ballabrera-Poy (2014), New blending algorithm to synergize ocean variables: The case of SMOS sea surface salinity maps (Liege Colloquium Special Issue: Remote sensing of ocean colour, temperature and salinity), *Remote Sens. Environ.*, *146*, 172–187, doi:10.1016/j.rse.2013.09.018.
Vinogradova, N. T., and R. M. Ponte (2013), Small-scale variability in sea surface salinity and implications for satellite-derived measurements, *J. Atmos. Oceanic Technol.*, *30*, 2689–2694, doi:10.1175/JTECH-D-13-00110.1.
Yin, X., J. Boutin, and P. Spurgeon (2013), Biases between measured and simulated SMOS brightness temperatures over ocean: Influence of Sun, *IEEE J. Selec. Top. Appl. Earth Observ. Remote Sens.*, *6*(3), 1341–1350, doi:10.1109/JSTARS.2013.2252602.
Yu, L. (2011), A global relationship between the ocean water cycle and near-surface salinity, *J. Geophys. Res.*, *116*, C10025, doi:10.1029/2010JC006937.
Zhang, H., G. Chen, C. Qian, and H. Jiang (2013), Assessment of two SMOS sea surface salinity level 3 products against Argo upper salinity measurements, *IEEE Trans. Geosci. Remote Sens. Lett.*, *10*(6), 1434–1438, doi:10.1109/LGRS.2013.2259792.